PHILOSOPHICAL TRANSACTIONS A

rsta.royalsocietypublishing.org

Research

Cite this article: Basu A, Chakrabarti BK. 2018 Hydrodynamic descriptions for surface roughness in fracture front propagation. *Phil. Trans. R. Soc. A* **377**: 20170387.
http://dx.doi.org/10.1098/rsta.2017.0387

Accepted: 6 August 2018

One contribution of 15 to a theme issue 'Statistical physics of fracture and earthquakes'.

Subject Areas:
statistical physics

Keywords:
hydrodynamics, fracture front propagation, scaling

Author for correspondence:
Abhik Basu
e-mail: abhik.basu@saha.ac.in; abhik.123@gmail.com

Hydrodynamic descriptions for surface roughness in fracture front propagation

Abhik Basu[1] and Bikas K. Chakrabarti[1,2]

[1]Condensed Matter Physics Division, Saha Institute of Nuclear Physics, Kolkata 700064, India
[2]S. N. Bose National Centre for Basic Sciences, Kolkata 700106, India

AB, 0000-0003-1048-6385

Fracture is ubiquitous in a crystalline material. Inspired by the observed phenomenological similarities between the spatial profile of a fractured surface and velocities in hydrodynamic turbulence, we set up a hydrodynamic description for the dynamics of fracture surface propagation mode I or opening fracture front. We consider several related continuum hydrodynamic models and use them to extract the similarities between the profile of a fractured surface and velocities in hydrodynamic turbulence. We conclude that a fractured surface should be generically self-similar with an underlying multifractal behaviour.

This article is part of the theme issue 'Statistical physics of fracture and earthquakes'.

1. Introduction

Fracture in crystalline media is a commonly observed phenomenon. It is now believed that profiles of fracture surfaces generically display robust universal scaling properties strongly reminiscent of fractal surfaces [1,2]. These in turn are visually similar to the velocity profiles observed in hydrodynamic turbulence [3]. Recent experimental studies [4] made quantitative estimates of the universal power laws in crack roughness statistics. These external similarities have led to the search for any deeper connections between the two apparently distant phenomena of fracture in crystalline media and hydrodynamic turbulence. A general hydrodynamic description of a fracture surface that directly brings out the underlying connections with hydrodynamic turbulence is lacking to date.

THE ROYAL SOCIETY PUBLISHING

Hydrodynamic approaches to condensed matter systems with slow modes and conserved densities have the advantages of being generic, i.e. independent of many microscopic details which appear as phenomenological parameters in the theory [5]. These are particularly well suited to extract the universal features in the long time, long wavelength limit [5]. Hydrodynamic theories for fluids have a long history of applications in driven systems (e.g. [6]). More recently, *smooth particle hydrodynamics*, a numerical method based on hydrodynamic approaches (e.g. [7]) have been applied to the various aspects of the fracture problem in mechanics, see [8] for recent applications. In this work, we set up the noisy continuum equations of motion for fracture surface propagation in the hydrodynamic limit. We focus on mode I or opening fracture front, where a tensile stress is applied normal to the plane of the crack. We consider several hydrodynamic models related to hydrodynamic turbulence. We show that in different limits the model equations formally resemble a range of well-known stochastically driven dynamical equations describing a moving Kardar–Parisi–Zhang surface (KPZ) [9] see also [10] with quenched disorder, passive scalar turbulence [11], magnetohydrodynamic (MHD) turbulence [12] and binary fluid turbulence [13]. We interpret the phenomenological similarities between a fracture surface and hydrodynamic surface in terms of these formal mathematical resemblances between the respective dynamical equations. The remainder of this article is organized as follows. In §2, we construct the equations of motion. We then analyse these equations and make correspondence with various models of hydrodynamic turbulence in §3. We finally conclude in §4.

2. Equations of motion

A opening fracture front in a crystalline medium starts propagating when the applied force exceeds a critical threshold that depends non-universally on the specific system under consideration. We begin by noting the generic experimentally observed feature that in a propagating fracture surface, not only there is a generic overall propagation along the direction of the applied force, also the fracture surface fluctuates normally to itself; see figure 1 for a schematic diagram of a moving opening fracture front.

We now consider the equations of motion of a mode I fracture front. We are interested in a long wavelength description in which a crystalline medium is described as a continuum elastic medium parametrized by the elastic constants. Now consider an elastic medium with a fracture surface in it. The instantaneous location of the fracture surface is given by the local distortion field $\mathbf{u}(\mathbf{x}, t)$, which are resolved into components along and perpendicular to the direction of fracture propagation $x_\parallel$; see figure 2 for a schematic geometry of the fracture surface.

Let us consider a propagating crack front (tip) and the corresponding equation for $\mathbf{v}_{\rm mat}$ of a small volume moving with the crack front. While the crack front moves on average with respect to the laboratory frame, in mode I or opening fracture front, the materials move in a direction normal to the fracture plane with a velocity $\mathbf{v}_{\rm mat}$. Thus, $\mathbf{v}_{\rm mat}$ is different from the average front velocity. From Newton's second law of motion, the momentum density $(\rho \mathbf{v}_{\rm mat})/t$ follows:

$$\rho \frac{\partial \mathbf{v}_{\rm mat}}{\partial t} = \mathbf{f}_v, \tag{2.1}$$

where $\mathbf{f}_v$ is the total force density including the external tensile stress, ρ is the local mass density at the crack front, assumed to be a constant for an incompressible material. In the steady state, the fracture front propagates essentially due to the longitudinal component of elastic restoring and other internal forces, but its motion gets hindered due to friction. On average, the friction balances the internal forces:

$$\langle \zeta \mathbf{v} \rangle = \langle \mathbf{F}_{\rm int} \rangle, \tag{2.2}$$

where $\langle \cdots \rangle$ refers to averaging over the noises (thermal and quenched; see below) in the system. Here, ζ is the friction coefficient. Here, $\mathbf{v} = (v_\parallel, \mathbf{v}_\perp)$ is the local velocity of the fracture front. It is observed that as the external tensile stress exceeds a threshold, the fracture front starts moving, and the in-plane fracture front velocity $v_\parallel$ has a non-zero average (above the threshold of the

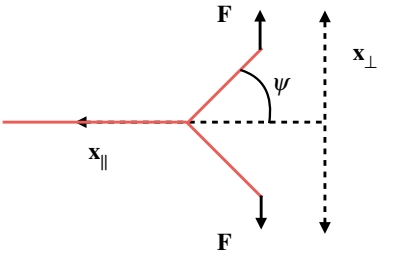

Figure 1. Schematic picture of a moving mode I or opening fracture front moving in the $x_\parallel$ (longitudinal) direction. The external pulling forces or tensile stress are applied are applied on each leaf in the $\mathbf{x}_\perp$ (transverse) direction. For simplicity of presentation, we have shown $x_\perp$ to be single component; in three dimensions $\mathbf{x}_\perp$ has two components, both in the directions normal to the direction of fracture front propagation. In the steady state, these are balanced by the normal component of the elastic restoring forces and other internal forces in each leaf. The net restoring force along the longitudinal direction is responsible for the motion of the fracture front, when it exceeds a threshold. We treat the angle ψ to be a constant. (Online version in colour.)

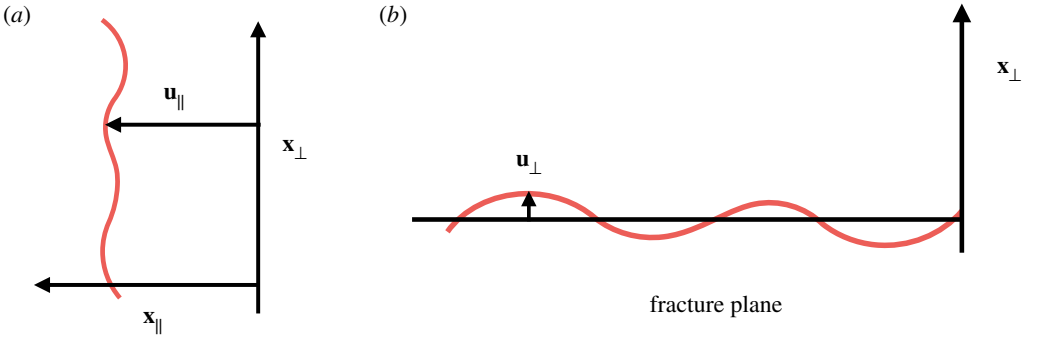

Figure 2. Definitions of (*a*) longitudinal displacement $u_\parallel$ (top view) and (*b*) transverse displacement $\mathbf{u}_\perp$ (front view); $\mathbf{u}_\perp$ represents local distortions from the undistorted position (i.e. the fracture plain) in directions normal to the fracture plane and is a two-dimensional vector in a three-dimensional system. (Online version in colour.)

pulling force). The internal forces include elastic forces, thermal noises and stochastic pinning forces (quenched disorders); the latter models the local defects in the underlying crystalline medium that acts as pinning centres for the fracture front.

The elastic restoring forces for a crystal in equilibrium originate from an elastic free energy. In order to simplify the presentation, we consider a single elastic constant A and assume an elastic free energy $\mathcal{F}_{\rm el} = \frac{1}{2}\int \mathrm{d}^d x A u_{ij}^2$, where $u_{ij} = (\partial_i u_j + \partial_j u_i)/2$ is the elastic strain tensor. Noting that the elastic stress tensor $\sigma_{ij}^{\rm el}$ is thermodynamic conjugate to u_{ij} [14], we have for the elastic stress tensor $\sigma_{ij}^{\rm el} = \delta\mathcal{F}_{\rm el}/\delta u_{ij} = A u_{ij}$ [14],[1] for an elastic medium in thermal equilibrium. The corresponding elastic force density is then given by $F_{{\rm int}i} = \nabla_j \sigma_{ij}^{\rm el} = A\nabla^2 u_i$, such that $\langle F_{{\rm int}i}\rangle = 0$. At the threshold of crack formations, the system is out of the elastic regime and also out of equilibrium. Thus, the equilibrium for the force density must be supplemented by nonlinear terms, which may not be obtained from a free energy. Furthermore, $\langle v_\parallel\rangle \sim \langle F_{{\rm int}\parallel}\rangle \neq 0$ for a propagating crack front moving along the $x_\parallel$-direction. The velocity of the local distortion by the definition $\partial\mathbf{u}/\partial t = \mathbf{v}$. We now resolve $\mathbf{u}$ as $\mathbf{u} = (u_\parallel, \mathbf{u}_\perp)$, where $u_\parallel$ and $\mathbf{u}_\perp$ are the components of $\mathbf{u}$ parallel and perpendicular to the direction of fracture propagation $\hat{x}_\parallel$. We set friction coefficient ζ to unity for simplicity. The

[1]We implicitly assume, in terms of the Maxwell model relating stresses with strain-rates, a large viscoelastic time-scale that is appropriate for a solid material.

general equation of motion for the fracture surface profile given by $\mathbf{u}$ is given by

$$\frac{\partial \mathbf{u}}{\partial t} = \mathbf{F}_{\text{int}}. \tag{2.3}$$

Here, $\mathbf{F}_{\text{int}}$ generically contains nonlinear terms whose forms may be fixed by symmetry considerations: all terms that are invariant under the symmetries of the system should be present. Note that the applied force $\mathbf{F}$, say along the $\hat{x}_\parallel$-direction, clearly distinguishes $+\hat{x}_\parallel$ from $-\hat{x}_\parallel$. Thus, no invariance is expected under $x_\parallel \to -x_\parallel$. There is no global rotational invariance due to the anisotropy introduced by the applied force. However, in the transverse $(d-1)$ dimensions, rotational invariance should hold. Considering the hydrodynamic limit and retaining up to the quadratic order nonlinear terms in $\mathbf{u}$, the equations of motion of $u_\parallel$ and $\mathbf{u}_\perp$ are of the generic form

$$\begin{aligned}\frac{\partial u_\parallel}{\partial t} &= B_\parallel \frac{\partial u_\parallel}{\partial x_\parallel} + A\nabla^2 u_\parallel + \tilde{B}_\parallel \boldsymbol{\nabla}_\perp \cdot \mathbf{u}_\perp + F_\parallel + \theta_\parallel(x_\parallel, \mathbf{x}_\perp) \\ &\quad + \lambda_{\parallel,1}\left(\frac{\partial u_\parallel}{\partial x_\parallel}\right)^2 + \lambda_{\parallel,2}\left(\frac{\partial u_\parallel}{\partial x_{\perp,m}}\right)^2 + \lambda_{\parallel,3}\left(\frac{\partial u_{\perp m}}{\partial x_{\perp,m}}\right)^2 + \lambda_{\parallel,4}(\boldsymbol{\nabla}_\perp \times \mathbf{u}_\perp)^2 + f_\parallel \end{aligned} \tag{2.4}$$

and

$$\begin{aligned}\frac{\partial \mathbf{u}_\perp}{\partial t} &= B_\perp \frac{\partial \mathbf{u}_\perp}{\partial x_\parallel} + \tilde{B}_\perp \frac{\partial u_\parallel}{\partial \mathbf{x}_\perp} + A\nabla^2 \mathbf{u}_\perp + \boldsymbol{\theta}_\perp(x_\parallel, \mathbf{x}_\perp) + \lambda_{\perp,1}\frac{\partial u_\parallel}{\partial x_{\perp,m}}\frac{\partial u_{\perp m}}{\partial \mathbf{x}_\perp} + \lambda_{\perp,2}\frac{\partial u_\parallel}{\partial x_{\perp,m}}\frac{\partial \mathbf{u}_\perp}{\partial x_{\perp,m}} \\ &\quad + \lambda_{\perp,3}\frac{\partial u_\parallel}{\partial \mathbf{x}_\perp}\frac{\partial u_{\perp m}}{\partial x_{\perp,m}} + \lambda_{\perp,4}\frac{\partial u_\parallel}{\partial x_\parallel}\frac{\partial \mathbf{u}_\perp}{\partial x_\parallel} + \mathbf{f}_\perp. \end{aligned} \tag{2.5}$$

In equations (2.4) and (2.5), stochastic functions $\mathbf{f}$ and $\boldsymbol{\theta}$ are thermal noise and quenched disorder, respectively. Here, only the most relevant terms in the hydrodynamic limit are included in (2.4) and (2.5). Furthermore, phenomenological parameters $\lambda_{\parallel,1}, \lambda_{\parallel,2}, \lambda_{\parallel,3}, \lambda_{\parallel,4}, \lambda_{\perp,1}, \lambda_{\perp,2}, \lambda_{\perp,3}, \lambda_{\perp,4}$ are the leading nonlinear coefficients, all of which have same scaling dimensions. Different parameters correspond to coupling between different modes. For systems with no handedness, the $\lambda_{\parallel,4}$-term should vanish. These nonlinear terms cannot be obtained from a free energy, but generically exist near a fracture front (see discussions above). Parameters $B_\parallel, \tilde{B}_\parallel, B_\perp, \tilde{B}_\perp$ set the speed of the propagating modes, or the growth rate of linearly unstable long wavelength modes, which may be generically present in the system. Stochastic functions $\boldsymbol{\theta}_\perp, \theta_\parallel$ are the quenched noises, $f_\parallel, \mathbf{f}_\perp$ are the thermal noises, $x_\parallel, \mathbf{x}_\perp$ are longitudinal and transverse coordinates. Quenched disorders $\boldsymbol{\theta}_\perp, \theta_\parallel$ and thermal noises $f_\parallel, \mathbf{f}_\perp$ are all assumed to be zero-mean, Gaussian-distributed with variances

$$\langle f_\parallel(\mathbf{x}, t) f_\parallel(0,0)\rangle = 2D_\parallel T\delta(\mathbf{x})\delta(t), \tag{2.6}$$

$$\langle f_{\perp i}(\mathbf{x}, t) f_{\perp j}(0,0)\rangle = 2D_\perp T\delta(\mathbf{x})\delta(t)\delta_{ij}, \tag{2.7}$$

$$\langle \theta_\parallel(\mathbf{x})\theta_\parallel(0)\rangle = 2\tilde{D}_\parallel \delta(\mathbf{x}) \tag{2.8}$$

and

$$\langle \theta_{\perp i}(\mathbf{x})\theta_{\perp j}(0)\rangle = 2\tilde{D}_\perp \delta(\mathbf{x})\delta_{ij}. \tag{2.9}$$

For an equilibrium system parameters $D_\parallel$ and $D_\perp$ which appear the variances of the thermal noises are fixed by the fluctuation dissipation theorem (FDT) [14] and are proportional to the kinetic coefficients (set to unity here) in equations (2.4) and (2.5), but are independent of the thermodynamic parameters like the elastic constants and temperature T. For an out of equilibrium system, there is no FDT and $D_\parallel$ and $D_\perp$ are formally to be treated as free parameters in our hydrodynamic theory. We expect them to depend on the microscopic model parameters as well as the conditions of the experiments; we are however unable to comment on any precise dependences. Formally, equations (2.4) and (2.5) describe time evolutions of the distortions in the longitudinal and transverse directions. Notice that equations (2.4) and (2.5) are all invariant under constant shifts $u_\parallel \to u_\parallel + u_\parallel^0$, $\mathbf{u}_\perp \to \mathbf{u}_\perp + \mathbf{u}_\perp^0$. This is consistent with the definition of $\mathbf{u}$ as the local distortions of the elastic medium. Equations (2.4) and (2.5) together provide the dynamical descriptions of the distortions $u_\parallel$ and $\mathbf{u}_\perp$.

3. Analysis of the model equations

Notice that

$$\left\langle \frac{\partial u_\parallel}{\partial t} \right\rangle = F_\parallel + \left\langle \lambda_{\parallel,1} \left(\frac{\partial u_\parallel}{\partial x_\parallel} \right)^2 \right\rangle + \lambda_{\parallel,2} \left\langle \left(\frac{\partial u_\parallel}{\partial x_{\perp,m}} \right)^2 \right\rangle + \lambda_{\parallel,3} \left\langle \left(\frac{\partial u_{\perp m}}{\partial x_{\perp,m}} \right)^2 \right\rangle + \lambda_{\parallel,4} \langle (\boldsymbol{\nabla}_\perp \times \mathbf{u}_\perp)^2 \rangle. \tag{3.1}$$

Thus, $\langle u_\parallel \rangle$ grows in time, consistent with the picture of a moving crack front moving along the $x_\parallel$-direction. The growth rate depends linearly upon $F_\parallel$ and receives nonlinear fluctuation corrections. By contrast, $\langle \partial_t \mathbf{u}_\perp \rangle = 0$, due to the linearity of equation (2.5) in $\mathbf{u}_\perp$, in agreement with the interpretation of $\mathbf{u}_\perp$ as the transverse fluctuations that is bounded in time. Here, $\langle .. \rangle$ implies averages over the distribution of the noises (both thermal and quenched). Physically interesting quantities include the spatio-temporal scaling of the correlation function of the longitudinal and transverse fluctuations

$$C_\parallel(\mathbf{r}, t) = \langle u_\parallel(\mathbf{r}, t) u_\parallel(0, 0) \rangle \tag{3.2}$$

and

$$C_\perp(\mathbf{r}, t) = \langle \mathbf{u}_\perp(\mathbf{r}, t) \cdot \mathbf{u}_\perp(0, 0) \rangle, \tag{3.3}$$

where $\mathbf{r} = (x_\parallel, \mathbf{x}_\perp)$. Recent experimental findings suggest that $C_\perp$ scales with spatial separations $\mathbf{r}$ [4]. Equivalently, one measures the widths of the fluctuations

$$w_\parallel(t) = \sqrt{\langle u_\parallel^2 \rangle - \langle u_\parallel \rangle^2} \tag{3.4}$$

and

$$w_\perp(t) = \sqrt{\langle \mathbf{u}_\perp^2 \rangle}, \tag{3.5}$$

which may be obtained from the knowledge of $C_\parallel$ and $C_\perp$. At the onset of crack propagation, $w_\parallel(t) \sim t^{\beta_\parallel}$, $w_\perp(t) \sim t^{\beta_\perp}$ and $w_\parallel \sim L^{\alpha_\parallel}$, $w_\perp \sim L^{\alpha_\perp}$; here L is the system size. Here, we implicitly assumed isotropic spatial scaling of $C_\parallel(\mathbf{r}, t)$ and $C_\perp(\mathbf{r}, t)$. However, given obvious anisotropy ($x_\parallel$ being the special direction), anisotropic spatial scaling is entirely possible. We however restrict ourselves to isotropic scaling for simplicity.

In the spirit of the well-known phenomenological Ginzburg–Landau approaches to universality near second-order phase transitions in equilibrium systems, these phenomenological parameters are formally treated as free parameters. Equations (2.4) and (2.5) are very general and do not correspond to any specific experimental realizations. Indeed, variation of these parameters should correspond to tuning experimental control parameters and/or microscopic material parameters. It is instructive to first consider the mode structure of the linearized versions of equations (2.4) and (2.5) in two dimensions (2d) (figure 2), for which the transverse component of $\mathbf{u}$ is $u_\perp$, just one-component quantity, $\mathbf{u} = (u_\parallel, u_\perp)$. The dispersion relation reads

$$\omega = \frac{[(B_\parallel + B_\perp) q_\parallel - 2\mathrm{i} A q^2 \pm \sqrt{(B_\parallel - B_\perp) q_\parallel^2 + \tilde{B}_\parallel \tilde{B}_\perp q_\perp^2}]}{2}, \tag{3.6}$$

where $\mathbf{q} = (q_\parallel, \mathbf{q}_\perp)$ is the wavevector, $q_\parallel$ is the component of $\mathbf{q}$ along the direction of crack propagation and $\mathbf{q}_\perp$ is the normal component; ω is the frequency. Thus, for $\tilde{B}_\parallel \tilde{B}_\perp > 0$ there are underdamped propagating modes at $O(q)$, where as for $\tilde{B}_\parallel \tilde{B}_\perp < 0$, there are linear instabilities at $O(q)$ (e.g. [15]). We do not know the sign of $\tilde{B}_\parallel \tilde{B}_\perp > 0$ *a priori* for a fracture front. However, given the absence of any experimental indications of unstable growth of fluctuations at the fracture surface, we neglect the possibility of linear instability and proceed further assuming linearly stable systems.

The nonlinear terms and the quenched noise rule out any exact treatment of the problem. Instead we take different limits and compare with the known results from the existing models.

(a) Different limits of the model

(i) Quenched Edward–Wilkinson equation

At the simplest level of analysis, we drop all nonlinear terms. Distortion components $u_\parallel$ and $\mathbf{u}_\perp$ then follow the following linear equations:

$$\frac{\partial u_\parallel}{\partial t} = B_\parallel \frac{\partial u_\parallel}{\partial x_\parallel} + \tilde{B}_\parallel \boldsymbol{\nabla}_\perp \cdot \mathbf{u}_\perp + A\nabla^2 u_\parallel + F_\parallel + \theta_\parallel(x_\parallel, \mathbf{x}_\perp) + f_\parallel \tag{3.7}$$

and

$$\frac{\partial \mathbf{u}_\perp}{\partial t} = B_\perp \frac{\partial \mathbf{u}_\perp}{\partial x_\parallel} + \tilde{B}_\perp \boldsymbol{\nabla}_\perp u_\parallel + A\nabla^2 \mathbf{u}_\perp + \theta_\perp + f_\perp. \tag{3.8}$$

Equations (3.7) and (3.8) remain coupled at the linear level through the spatial first derivative cross terms, corresponding to a dispersion relation given by (3.6). Even with linear stability, (3.6) does not allow for a simple decoupling of (3.7) and (3.8) into two linear equations for arbitrary $q_\parallel$ and $\mathbf{q}_\perp$. We now make further simplifying approximation and set $\tilde{B}_\parallel = 0 = \tilde{B}_\perp$, which implies that the spatial variations of $u_\parallel$ along $\mathbf{x}_\perp$ direction does not affect the local distortion of $\mathbf{u}_\perp$ and vice versa. This approximation decouples equations (3.7) and (3.8). The individual wave-like terms in (3.7) and (3.8) can be absorbed separately by going to the respective comoving frames, which make both (3.7) and (3.8) take the standard form of the linear Edward–Wilkinson (EW) equation with quenched disorder [16], that is studied extensively in the literature, shows roughening phenomena that is controlled by the quenched disorder. Given the fact that linear equations (3.7) and (3.8) are essentially coupled generalizations of the standard quenched EW equation, the former equations should also display roughening phenomena. In the special limit $\tilde{B}_\parallel = 0$, $u_\parallel$ follows the standard quenched EW equation (after removing the $B_\parallel$-term by comoving). The statistical properties of $u_\parallel$ are known in this limit [16]. In this limit, the dynamics of $\mathbf{u}_\perp$ as given by (3.8) clearly has $u_\parallel$ in it through $\tilde{B}_\perp$-term. The latter contribution may be interpreted as an additional *additive* noise with a statistics determined by the quenched EW equation. This is going to alter the statistics of roughening of $\mathbf{u}_\perp$ from its EW limit ($\tilde{B}_\perp = 0$). Consider now the general case, in the where none of $\tilde{B}_\parallel$ and $\tilde{B}_\perp$ vanish. In the comoving frame of $\mathbf{u}_\perp$, the $B_\perp$-term in (3.8) disappears, and the $u_\parallel$-fluctuations in this frame are primarily wave-like, leading to make them subdominant to the corresponding $\mathbf{u}_\perp$ fluctuations. This is expected to make the $\tilde{B}_\perp$-term in (3.8) irrelevant in a scaling sense [17]. This should then restore the standard quenched EW scaling for $\mathbf{u}_\perp$ [16]. Similar arguments yield the same quenched EW scaling for $u_\parallel$-fluctuations. Overall thus, our discussions here are consistent with the observed roughness of the transverse fluctuations in a moving fracture front.

(b) Quenched Kardar–Parisi–Zhang equation

In the next step, we set couplings $\tilde{B}_\parallel, \lambda_\parallel, \lambda_{\parallel,4}$ to zero, rescale $\mathbf{x}_\perp$ and $x_\parallel$ to make $\lambda_{\parallel,1} = \lambda_{\parallel,2}$, absorb the propagating wave (the $B_\parallel$-term) by co-moving, or equivalently by a Galilean transformation. Then identifying $u_\parallel$ with a height h, we obtain

$$\frac{\partial h}{\partial t} = A\nabla^2 h + \lambda_{\parallel,1}\left(\frac{\partial h}{\partial x_m}\right)^2 + \theta_\parallel + f_\parallel. \tag{3.9}$$

This is the usual quenched KPZ equation [16,18,19]. It was expected that the scaling of the roughening transition equation (3.9) should be in the same universality class as the quenched EW equation, since the KPZ nonlinearity that is formally absent in the quenched EW equation should be automatically generated in the latter due to the highly non-trivial dependence of the quenched disorder on h [18,19]. However, several detailed studies indicated that the universal properties of the roughening transition in the quenched KPZ equation are different from those in the quenched EW equation [16,18,19]. Dimensional arguments as reported in [18,19] yield exponents $\alpha_\parallel = (4-d)/4$, $\beta_\parallel = (4-d)/(4+d)$ in d-dimensions. In this limit, the dynamics of $\mathbf{u}_\perp$ as given by

equation (2.5) is driven by $u_\perp$ that appears as a *multiplicative noise*, whose statistics is determined by the quenched KPZ equation. Note that, regardless of the nature of the solutions, the structure of equation (2.5) ensures that $\langle \partial \mathbf{u}_\perp / \partial t \rangle = 0$. This follows from the fact that (a) equation (2.5) is linear in $\mathbf{u}_\perp$ implying invariance under $\mathbf{u}_\perp \to -\mathbf{u}_\perp$. Thus, $\langle \mathbf{u}_\perp \rangle$ should be *bounded*, unlike $\langle u_\parallel \rangle$, which continuously grows, reflecting the average motion of the crackfront in the longitudinal direction. We are interested in the scaling of $\mathbf{u}_\perp$. As in (3.7) and (3.8), notice that with $B_\parallel \neq B_\perp$, wave terms in both (2.4) and (2.5) cannot be removed. Equivalently, there is *no* frame where both the waves vanish.

Notice the formal similarity (in the mathematical structure) of equation (2.4) the Navier–Stokes equation for fluid flows and the Burgers equation for pressureless fluids (related to the KPZ equation). Then, in analogy with the studies on fluid turbulence and depinning of contact lines, for sufficiently large applied force $F_\parallel$ above the threshold of depinning, $u_\parallel(\mathbf{x}, t)$ *is turbulent*, i.e. the equal-time correlator $\langle [u_\parallel(\mathbf{x}, t) - u_\parallel(\mathbf{x}', t)]^2 \rangle$ scale qualitatively similarly with the same for the velocity in fluid turbulence. Thus, $u_\parallel(\mathbf{x}, t)$ should be a *long-range* field. Now in the limit, when $u_\parallel$ is autonomous, it appears as a *long-range* noise in the equation for $\mathbf{u}_\perp(\mathbf{x}, t)$. For simplicity, set the quenched disorder $\boldsymbol{\theta}_\perp(x_\parallel, \mathbf{x}_\perp)$ to zero.

$$\frac{\partial \mathbf{u}_\perp}{\partial t} = B_\perp \frac{\partial \mathbf{u}_\perp}{\partial x_\parallel} + A\nabla^2 \mathbf{u}_\perp + \lambda_{\perp,1} \frac{\partial u_\parallel}{\partial x_{\perp,m}} \frac{\partial u_{\perp m}}{\partial \mathbf{x}_\perp} + \lambda_{\perp,2} \frac{\partial u_\parallel}{\partial x_{\perp,m}} \frac{\partial \mathbf{u}_\perp}{\partial x_{\perp,m}} + \lambda_{\perp,3} \frac{\partial u_\parallel}{\partial \mathbf{x}_\perp} \frac{\partial u_{\perp m}}{\partial x_{\perp,m}} + \lambda_{\perp,4} \frac{\partial u_\parallel}{\partial x_\parallel} \frac{\partial \mathbf{u}_\perp}{\partial x_\parallel} + \mathbf{f}_\perp. \tag{3.10}$$

In that limit, we draw analogy with the well-known passive scalar problem of fluid turbulence, where a scalar field c (smoke density, local temperature) is advected by a turbulent velocity field:

$$\frac{\partial c}{\partial t} + \mathbf{v} \cdot \boldsymbol{\nabla} c = D_c \nabla^2 c + \theta_c. \tag{3.11}$$

Here, $\mathbf{v}$ is an incompressible velocity field, D_c is the diffusivity and θ_c is a conserved noise [20–26] Equation (3.11) has been studied in details and is found to show turbulent-like behaviour. It is known that all even-order equal-time structure functions $S_p(r) = \langle [c(\mathbf{x} + \mathbf{r}, t) - c(\mathbf{x})]^{2p} \rangle \sim r^{\zeta_p}$, where ζ_p is a nonlinear function of p. This is known as *multiscaling* in the turbulence literature [3]. Drawing on the formal similarities between $\mathbf{v}$ in (3.11) and spatial gradients of $u_\parallel$ in (3.10), we expect $\mathbf{u}_\perp(\mathbf{x}, t)$ to be long-range as well, i.e. it should also show turbulent behaviour. So far we have ignored the quenched disorder $\boldsymbol{\theta}_\perp$, which is another source of randomness that is *independent* of time. Averaging over the distribution of $\boldsymbol{\theta}_\perp$ should yield the experimentally accessible scaling of the correlation function of $\mathbf{u}_\perp$. Given that $\mathbf{u}_\perp$-correlators in (3.10) generically display long-range correlations, it can be reasonably claimed that quenched-disorder averaged correlator of $\mathbf{u}_\perp$ also displays long-range behaviour, or *turbulence* like scaling. In the special limit $\tilde{B}_\parallel = 0 = \tilde{B}_\perp$, noting that the naive scaling dimensions of $u_\parallel$ and $\mathbf{u}_\perp$ should be same (this can be argued from simple power counting reasons), simple extension of the dimensional arguments of [18,19] suggests $\alpha_\parallel = \alpha_\perp$ and $\beta_\parallel = \beta_\perp$. For other choices of $\tilde{B}_\parallel$, $\tilde{B}_\perp$ the scaling exponents of $u_\parallel$ should stay unchanged following the arguments we have given in the previous subsection. However, the exponents $\alpha_\perp$, $\beta_\perp$ should change. The precise values of these scaling exponents cannot be obtained easily from dimensional arguments.

(c) The general case

Now, the above argument rests on the assumption of $u_\parallel(\mathbf{x}, t)$ being autonomous, which in general is not true. When the other couplings, e.g. $\lambda_{\parallel_3}$, are non-zero, $u_\parallel$ should still become rough when $F_\parallel$ exceeds a threshold, which may now depend on the additional coupling constants. Again ignore

the quenched disorders for simplicity. Variable $u_\parallel$ now follows the equation:

$$\frac{\partial u_\parallel}{\partial t} = B_\parallel \frac{\partial u_\parallel}{\partial x_\parallel} + A\nabla^2 u_\parallel + F_\parallel + \lambda_{\parallel,1}\left(\frac{\partial u_\parallel}{\partial x_\parallel}\right)^2 + \lambda_{\parallel,2}\left(\frac{\partial u_\parallel}{\partial x_{\perp,m}}\right)^2 + \lambda_{\parallel,3}\left(\frac{\partial u_{\perp m}}{\partial x_{\perp,m}}\right)^2 + \lambda_{\parallel,4}(\boldsymbol{\nabla}_\perp \times \mathbf{u}_\perp)^2 + f_\parallel, \tag{3.12}$$

with $\mathbf{u}_\perp$ still follows (3.10). We now notice the similarities between the pair of equations (3.12) and (3.10), and those which govern binary fluid turbulence [11], or magnetohydrodynamic (MHD) turbulence [12]. For instance, the MHD equations for the velocity $\mathbf{v}$ and the magnetic field $\mathbf{b}$ are given by

$$\frac{\partial \mathbf{v}}{\partial t} + \lambda_1 \mathbf{v}.\nabla\mathbf{v} = -\frac{\nabla p}{\rho} + \lambda_2 \frac{(\nabla \times \mathbf{b}) \times \mathbf{b}}{4\pi\rho} + \nu\nabla^2\mathbf{v} + \mathbf{f}_v \tag{3.13}$$

with $\nabla.\mathbf{v} = 0$ since we consider an incompressible fluid; and Ampère's law for a conducting fluid becomes

$$\frac{\partial \mathbf{b}}{\partial t} + \lambda_3 \mathbf{v}.\boldsymbol{\nabla}\mathbf{b} = \lambda_3 \mathbf{b}.\boldsymbol{\nabla}\mathbf{v} + \eta\nabla^2\mathbf{b} + \mathbf{f}_b, \tag{3.14}$$

which is to be supplemented by Maxwell's equation $\boldsymbol{\nabla}.\mathbf{b} = 0$. Here, $\lambda_1, \lambda_2, \lambda_3$ are the nonlinear coupling constants. A pair of equations for scalar c and velocity $\mathbf{v}$ having formally similar structures as the MHD equations (3.13) and (3.14) govern the dynamics of binary fluid turbulence. It is well known that both binary fluid and MHD turbulence display turbulence-like behaviour for sufficiently strong external forces. In fact all the relevant dynamical variables $\mathbf{v}$, $\mathbf{b}$ and c display multiscaling [13,27]. With that analogy in mind, it may be concluded that both $u_\parallel$ and $\mathbf{u}_\perp$ should display turbulence-like behaviour. Thus, it is reasonable to expect that even with the couplings with $\mathbf{u}_\perp$, $u_\parallel$ should show turbulent-like behaviour for sufficiently large $F_\parallel$. This in turn should imply, via the coupling of $\mathbf{u}_\perp$ with $u_\parallel$ in equation (2.5) that $\mathbf{u}_\perp$ should show turbulent behaviour for sufficiently large pulling forces. Then again with the quenched disorders included, both $u_\parallel$ and $\mathbf{u}_\perp$ should continue to display multiscaling that generalizes the scaling displayed by $w_\parallel$ and $w_\perp$: Our specific suggestions include measurements of

$$S_{u_\parallel}(r) = \langle [u_\parallel(\mathbf{x}+\mathbf{r},t) - u_\parallel(\mathbf{x},t)]^n \rangle \sim r^{\zeta_n^\parallel} \tag{3.15}$$

and

$$S_{u_\perp}(r) = \langle [|\mathbf{u}_\perp(\mathbf{x}+\mathbf{r},t) - \mathbf{u}_\perp(\mathbf{x},t)|^n] \rangle \sim r^{\zeta_n^\perp}, \tag{3.16}$$

with $\zeta_n^\parallel$ and $\zeta_n^\perp$ being nonlinear functions of n that are expected to depend on the distributions of the quenched disorder $\theta_\parallel$ and $\boldsymbol{\theta}_\perp$. These scaling behaviours connect the phenomenon of fracture with hydrodynamic turbulence. Analytical enumeration of these exponents remain elusive till today. We expect high-resolution numerical simulations should be able to measure these exponents accurately. Any extension of the dimensional arguments of [18,19] becomes difficult due to the presence of several nonlinearities having the same naive scaling dimensions. Studying how these different nonlinear terms that are equally relevant in a scaling sense affect the scaling exponents remains a challenging theoretical task. Nonetheless, we can make the following general comments: (i) both the longitudinal and transverse components of the local displacements in a fracture front should be multifractal or display multiscaling, akin to the velocity field in hydrodynamic turbulence. (ii) We suggest experimental measurements of scaling by the structure function of $u_\parallel$ and $\mathbf{u}_\perp$ as defined above in (3.15) and (3.16). (iii) We expect the different nonlinear coupling constant in the dynamical equations (2.4) and (2.5) to be functions of the microscopic parameters that characterize different materials. Thus, controlled experiments with different materials should help delineate different universality classes.

4. Summary and outlook

In this work, we have proposed several related hydrodynamic models for fracture surface propagation in mode I or opening fracture front. We show that different specific limits of our

model equations resemble well-known dynamical models with quenched disorder, e.g. quenched EW equation or quenched KPZ equation. By drawing analogy with the hydrodynamic models for a hosts of hydrodynamic phenomena ranging from passive scalar turbulence to binary fluid and MHD turbulence, we argue that the spatial profile for the local distortion field **u** in a moving fracture surface should display multiscaling or equivalently multifractal, akin to the velocity profiles in hydrodynamic turbulence. Since the stress σ_{ij} should have complex dependences on the strain u_{ij} (possibly in a nonlinear manner for fracture), multifractality for **u** naturally indicates multifractal behaviour for the local stress, although the multifractality of u_{ij} is not expected to be simply related to the multifractality of σ_{ij}. It will thus be interesting to study the scaling behaviours of the correlation or structure functions of the stress as well and investigate how that correlate with the observed universality of the fracture fronts.

Our model equations contain several phenomenological coupling parameters, e.g. $B_\parallel, \tilde{B}_\parallel, B_\perp, \tilde{B}_\perp, \lambda_{\parallel,1}, \lambda_{\parallel,2}, \lambda_{\parallel,3}, \lambda_{\parallel,4}, \lambda_{\perp,1}, \lambda_{\perp,2}, \lambda_{\perp,3}, \lambda_{\perp,4}$, all of which are assumed to be free parameters in our model equations. For actual samples, these phenomenological parameters should depend upon the microscopic structure (e.g. the crystal structure) and microscopic interactions between the crystalline material and the fracture forces, which may be studied in terms of atomistic descriptions. Given the dependence of the macroscopic behaviour on the coupling constants as elucidated above, we expect different materials and/or different forcing mechanisms should yield macroscopically different fracture surface profiles. Detailed quantitative studies, perturbative analytical or numerical, along those lines by using our model equations should be welcome. Similar to fluid turbulence and other related systems, it is expected that the multifractal behaviour of **u** should be independent of the precise numerical values of the various parameters introduced above, which is the essence of universality here. It is however possible that different dimensionless ratios of the model parameters actually classify the different universality classes of fracture fronts, something we are unable to comment on from the analysis above. More detailed calculations or numerical studies of the relevant models should be able to shed light on this. In our analyses, we have neglected the possibilities of multiplicative quenched disorders that are known to generate new universal properties close to some experimental results [18,19,28,29]. It will be interesting to see how such disorders may affect our analyses above. It will also be interesting to see how our analysis here can be extended to other modes of fracture front, e.g. mode II and mode III.

Data accessibility. This article has no additional data.

Authors' contributions. Both the authors jointly formulated the problem, carried the analysis and wrote the manuscript.

Competing interests. We declare we have no competing interests.

Funding. A.B. gratefully acknowledges partial financial support from the Alexander Von Humboldt Stiftung (Germany) through the Research Group Linkage Programme (2016). B.K.C. acknowledges DST (India) for support from a J. C. Bose Fellowship.

References

1. Mandelbrot BB, Passoja DE, Paullay AJ. 1984 Fractal character of fracture surfaces of metals. *Nature* (*London*) **308**, 721–722. (doi:10.1038/308721a0)
2. Bonamy D, Bouchaud E. 2011 Failure of heterogeneous materials: a dynamic phase transition? *Phys. Rep.* **498**, 1–44. (doi:10.1016/j.physrep.2010.07.006)
3. Frisch U. 1995 *Turbulence: the legacy of A.N. Kolmogorov*. Cambridge, UK: Cambridge University Press.
4. Vernède S, Ponson L, Bouchaud J-P. 2015 Turbulent fracture surfaces: a footprint of damage percolation? *Phys. Rev. Lett.* **114**, 215501. (doi:10.1103/PhysRevLett.114.215501)
5. Martin PC, Parodi O, Pershan PS. 1972 Unified hydrodynamic theory for crystals, liquid crystals, and normal fluids. *Phys. Rev. A* **6**, 2401–2420. (doi:10.1103/PhysRevA.6.2401)
6. Forster D, Nelson DR, Stephen MJ. 1977 Large-distance and long-time properties of a randomly stirred fluid. *Phys. Rev. A* **16**, 732–749. (doi:10.1103/PhysRevA.16.732)

7. Monaghan JJ. 1992 Smoothed particle hydrodynamics. *Annu. Rev. Astron. Astrophys.* **30**, 543–574. (doi:10.1146/annurev.aa.30.090192.002551)
8. Douillet-Grellier T, Jones BD, Pramanik R, Pan K, Albaiz A, Williams JR. 2016 Mixed-mode fracture modeling with smoothed particle hydrodynamics. *Comput, Geotechnics* **79**, 73–85. (doi:10.1016/j.compgeo.2016.06.002)
9. Kardar M, Parisi G, Zhang Y-C. 1986 Dynamic scaling of growing interfaces. *Phys. Rev. Lett.* **56**, 889–892. (doi:10.1103/PhysRevLett.56.889)
10. Barabasi A-L, Stanley HE. 1995 *Fractal concepts in surface growth*. Cambridge, UK: Cambridge University Press.
11. Ruiz R, Nelson DR. 1981 Turbulence in binary fluid mixtures. *Phys. Rev. A* **23**, 3224–3246. (doi:10.1103/PhysRevA.23.3224)
12. Biskamp D. 1993 *Nonlinear magnetohydrodynamics*. Cambridge, UK: Cambridge University Press.
13. Ray SS, Basu A. 2011 Universality of scaling and multiscaling in turbulent symmetric binary fluids. *Phys. Rev. E* **84**, 036316. (doi:10.1103/PhysRevE.84.036316)
14. Chaikin PM, Lubensky TC. 2000 *Principles of condensed matter physics*. Cambridge, UK: Cambridge University Press.
15. Lahiri R, Ramaswamy S. 1997 Are steadily moving crystals unstable? *Phys. Rev. Lett.* **79**, 1150–1153. (doi:10.1103/PhysRevLett.79.1150)
16. Amaral LAN, Barabá?si A-L, Makse HA, Stanley HE. 1995 Scaling properties of driven interfaces in disordered media. *Phys. Rev. E* **52**, 4087–4104. (doi:10.1103/PhysRevE.52.4087)
17. Das D, Basu A, Barma M, Ramaswamy S. 2001 Weak and strong dynamic scaling in a one-dimensional driven coupled-field model: effects of kinematic waves. *Phys. Rev. E* **64**, 021402. (doi:10.1103/physreve.64.021402)
18. Csahok Z, Honda K, Vicsek T. 1993 Dynamics of surface roughening in disordered media. *J. Phys. A: Math. Gen.* **26**, L171–L178. (doi:10.1088/0305-4470/26/5/001)
19. Csahók Z, Honda K, Somfai E, Vicsek M, Vicsek T. 1993 Dynamics of surface roughening in disordered media. *Physica A* **200**, 136–154. (doi:10.1016/0378-4371(93)90512-3)
20. Kraichnan RH. 1994 Anomalous scaling of a randomly advected passive scalar. *Phys. Rev. Lett.* **72**, 1016–1019. (doi:10.1103/PhysRevLett.72.1016)
21. Gawedzki K, Kupiainen A. 1995 Anomalous scaling of the passive scalar. *Phys. Rev. Lett.* **75**, 3834–3837. (doi:10.1103/PhysRevLett.75.3834)
22. Adzhemyan LTs, Antonov NV, Vasilev AN. 1998 Renormalization group, operator product expansion, and anomalous scaling in a model of advected passive scalar. *Phys. Rev. E* **58**, 1823–1835. (doi:10.1103/PhysRevE.58.1823)
23. Chertkov M, Falkovich G, Kolokolov I, Lebedev V. 1995 Normal and anomalous scaling of the fourth-order correlation function of a randomly advected passive scalar. *Phys. Rev. E* **52**, 4924–4941. (doi:10.1103/PhysRevE.52.4924)
24. Chertkov M, Falkovich G. 1996 Anomalous scaling exponents of a white-advected passive scalar. *Phys. Rev. Lett.* **76**, 2706–2709. (doi:10.1103/PhysRevLett.76.2706)
25. Bernard D, Gawedzki K, Kupiainen A. 1996 Anomalous scaling in the *N*-point functions of a passive scalar. *Phys. Rev. E* **54**, 2564–2572. (doi:10.1103/PhysRevE.54.2564)
26. Banerjee T, Basu A. 2018 Perspectives on scaling and multiscaling in passive scalar turbulence. (http://arxiv.org/abs/1801.00998)
27. Basu A, Sain A, Dhar SK, Pandit R. 1998 Multiscaling in models of magnetohydrodynamic turbulence. *Phys. Rev. Lett.* **81**, 2687–2690. (doi:10.1103/PhysRevLett.81.2687)
28. Horváth VK, Family F, Vicsek T. 1991 Dynamic scaling of the interface in two-phase viscous flows in porous media. *J. Phys. A* **24**, L25–L29. (doi:10.1088/0305-4470/24/1/006)
29. Horváth VK, Family F, Vicsek T. 1991 Anomalous noise distribution of the interface in two-phase fluid flow. *Phys. Rev. Lett.* **67**, 3207–3210. (doi:10.1103/physrevlett.67.3207)